Journal of Power Sources 226 (2013) 20–26

Contents lists available at SciVerse ScienceDirect

Journal of Power Sources

journal homepage: www.elsevier.com/locate/jpowsour

Enhanced electrochemical performances of $LiFePO_4$/C by surface modification with Sn nanoparticles

Yingbin Lin*, Ying Lin, Ting Zhou, Guiying Zhao, Yandan Huang, Zhigao Huang**

College of Physics and Energy, Fujian Normal University, Fuzhou 350007, China

HIGHLIGHTS

- With Sn-coating, the electrochemical performance of $LiFePO_4$ is improved in a wide operation temperature.
- Metallic Sn layer suppresses the Fe dissolution and reduce the charge-transfer resistance.
- High conductive Sn facilitates the kinetics for lithium diffusion at low temperature.

ARTICLE INFO

Article history:
Received 8 August 2012
Received in revised form
28 September 2012
Accepted 22 October 2012
Available online 29 October 2012

Keywords:
Li-ion battery
Lithium iron phosphate
Rate performance
Cyclability
Surface modification

ABSTRACT

The surface of $LiFePO_4$/C cathode material is coated with nano-sized Sn via a simple electroless deposition (ED) process, and the effects of the Sn-coating on the electrochemical performances of $LiFePO_4$/C are investigated systematically by the charge/discharge testing, cyclic voltammograms and AC impedance spectroscopy, respectively. In comparison with the pristine $LiFePO_4$/C, the Sn-coated $LiFePO_4$/C exhibits higher capacity, better cyclability and higher rate capability in a wide operation temperature range. An analysis of the electrochemical measurements reveals that Sn-coated $LiFePO_4$/C has good electric contact among particles, much lower charge-transfer resistances and higher lithium diffusion rate, especially at low temperature. In addition, the Sn-coating layer protects the active materials from chemical attack by HF and thus suppresses the dissolution of Fe from $LiFePO_4$ in the $LiPF_6$ based electrolyte.

1. Introduction

Recently, great interest has arisen in application of olivine-structured orthophosphates $LiFePO_4$ as cathode materials for lithium-ion secondary batteries due to its flat voltage profile and high theoretical capacity (170 mAh g^{-1}) as well as low cost and environment benignity [1–4], all of which was considered to promote application of plug-in hybrid vehicle [5]. However, the low intrinsic electronic conductivity ($\sim 10^{-8}$–10^{-10} S cm^{-1}) and lithium-ion diffusivity ($\sim 10^{-18}$ cm^2 s^{-1}) of $LiFePO_4$ have been major obstacles to electrochemical extraction of lithium and results in steep falling in capacity at high rates [6,7].

Tremendous efforts have been devoted to improvement of electrochemical performances of olivine $LiFePO_4$ and the surface coating with a more conductive material including carbon and Ag is well-known as an effective way in improving the rate performance of $LiFePO_4$ cathode [8–12]. For instance, Mi et al. [8] have revealed that the surface modification of $LiFePO_4$ with silver and carbon demonstrates obviously enhanced rate capability and improved capacity retention rate. Song et al. [9] have reported that the surface modified $LiFePO_4$ by NiP exhibits significantly enhanced electrochemical reversibility and stability at elevated temperature.

Metallic Sn with high electronic conductivity seems to be a promising alternative coating-material for improving rate capability due to its facile fabrication and low cost. Combining the above ideas, composing $LiFePO_4$ with both carbon-webs and metallic Sn would be reasonably beneficial for improved rate capability and cyclic reversibility due to the formation of an integrate network on the bare surface of $LiFePO_4$ particles, which not only provides a highly conductive nanolayer between particles but also protects the active materials from chemical attack by HF in electrolyte. In present work, a simple electroless deposition method is employed to deposit the uniform distribution of nano-sized Sn particles on the surface of $LiFePO_4$/C particles. Compared to the pristine $LiFePO_4$/C, the as-prepared $LiFePO_4$/C–Sn exhibits superior electrochemical performances in a wide operation temperature range.

* Corresponding author. Tel./fax: +86 591 2286 8132.
** Corresponding author. Tel./fax: +86 591 2286 7577.
E-mail addresses: yblin@fjnu.edu.cn (Y. Lin), zghuang@fjnu.edu.cn (Z. Huang).

0378-7753/$ – see front matter © 2012 Elsevier B.V. All rights reserved.
http://dx.doi.org/10.1016/j.jpowsour.2012.10.074

2. Experimental

2.1. Preparation and characterization of cathode materials

Carbon coated $LiFePO_4$ composite materials were first prepared by a carbothermal reduction method. In detail, analytical grade $LiCH_3COO{\cdot}2H_2O$, $FeC_2O_4{\cdot}2H_2O$, and $NH_3H_2PO_4$ in stoichiometric amounts were thoroughly planetary milled in mortar for 12 h in ethanol containing proper amount of sucrose as carbon source. The obtained slurry was dried at 60 °C in an oven and then pressed into pellets. These pellets were transferred to a temperature-controlled tube furnace equipped with flowing Ar gas and calcined at 350 °C for 3 h and subsequently sintered at 700 °C for 12 h to obtain $LiFePO_4$ coated with carbon (denoted as $LiFePO_4$/C). Nano-sized Sn was deposited on $LiFePO_4$/C particles through an ED approach. In detail, the as-prepared $LiFePO_4$/C powder was ultrasonically dispersed in absolute ethanol containing an appropriate amount of $SnCl_2$middot$2H_2O$. After being stirred for 3 h, sodium borohydride ($NaBH_4$) solution in a molar ratio of 1:7 to $SnCl_2$ was added into the above suspension drop by drop under vigorous stirring. The reactant precursors were kept stirring for 12 h to drive the reduction of Sn^{2+} on $LiFePO_4$/C particles. The obtained precipitates were washed several times with deionized water and ethanol, and subsequently dried at 70 °C in vacuum to get the final product (denoted as $LiFePO_4$/C–Sn). The phase identification of the pristine $LiFePO_4$/C and $LiFePO_4$/C–Sn powders was conducted with an X-ray diffractometer (XRD, Rigaku MiniFlex II) using CuK_α radiation ($\lambda = 0.15405$ nm). The morphology of the composites was studied with a scanning electron microscope (SEM, JSM-7500F, Japan) equipped with an energy dispersive spectroscope (EDS). The nanoscale microstructure of $LiFePO_4$/C–Sn particles was examined using a transmission electron microscope (TEM, Tecnai G2 F20 S-TWIN).

2.2. Cell fabrication and characterization

The working electrode was prepared by homogeneously pasting a slurry containing 80 wt.% active material, 10 wt.% super-P and 10 wt.% polyvinylidene fluoride (PVDF) dissolved in *N*-methyl-2-pyrrolidone on an Al foil and subsequently dried in vacuum at 110 °C over night. The coin cells (R2025) were assembled in an argon-filled glove box (Mikrouna, Super 1220/750, China) with Li metal as anode and counter electrode, Celgard 2300 microporous polyethylene membrane as separator and 1 M $LiPF_6$ in a mixture of ethyl carbonate (EC) and dimethyl carbonate (DMC) (1:1 in vol. ratio) as electrolyte. Galvanostatic charge/discharge measurements were carried out in the voltage range of 2.0–4.5 V with a CT2001A cell test instrument (LAND Electronic Co.). Cyclic voltammograms (CV) and electrochemical impedance spectra (EIS) measurements were performed by Arbin 2000 testing system and electrochemical workstation (CHI660C) respectively. The CV measurement was carried out between 2.0 and 4.5 V, and the EIS analysis was recorded in a frequency range from 10 mHz to 100 kHz with an amplitude of 5 mV. Electrical properties were measured by a Versalab magnetometer (Versalab free, Quantum Design Co.). The dissolved amounts of transition metal elements were analyzed by inductively coupled plasma OES spectrometer (ICP, Ultima 2, Jobin Yvon).

3. Results and discussion

3.1. Material characterization

Fig. 1 shows XRD patterns of the pristine and $LiFePO_4$/C–Sn powders. All the observed diffraction peaks for pristine powder can be indexed well based on an olivine-type phase structure with a space group of Pmnb (JCPDS No. 40-1499), indicating the successful synthesis of phase-pure $LiFePO_4$. The diffraction pattern of $LiFePO_4$/C–Sn is identical to those of the pristine sample, even though a modification layer on the surface. Besides the main $LiFePO_4$ olivine phase, an additional diffraction peak is also observed, which corresponds to the (200) reflection of tetragonal Sn (JCPDS No. 65-2631).

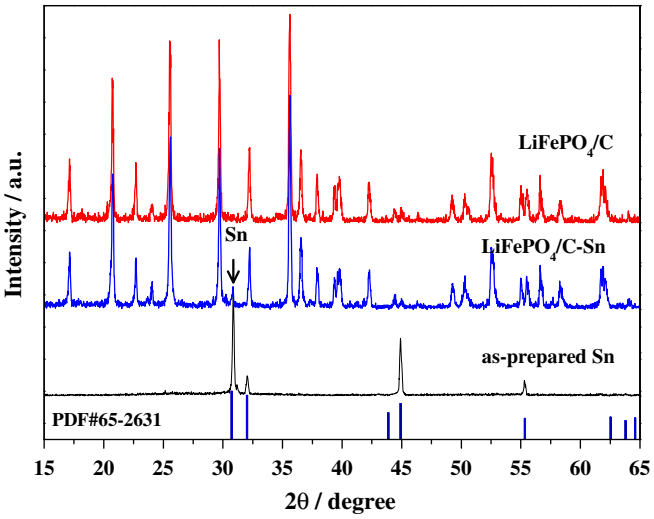

Fig. 1. XRD patterns of the as-prepared $LiFePO_4$/C and $LiFePO_4$/C–Sn powders.

Fig. 2(a) and (b) presents the surface morphologies examined by SEM for the pristine and $LiFePO_4$/C–Sn composites, respectively. In comparison with the pristine $LiFePO_4$/C, nano-sized Sn particles are uniformly dispersed on the $LiFePO_4$/C surface. Such homogeneous Sn-coating is expected to form conducting network between particles and prevents Fe^{2+} dissolution from $LiFePO_4$, resulting in a superior discharge/charge performance. The elemental EDS analysis of the surface layer for $LiFePO_4$/C–Sn is present in Fig. 2(c). Analysis of EDS results confirm the presence of Sn on the $LiFePO_4$ and the corresponding content of Sn is approximately estimated as 4 wt.%. The nanoscale microstructure of the $LiFePO_4$/C–Sn is further studied by the transmission electron microscopy (TEM). As shown in Fig. 3, nano-sized Sn particles with an average diameter of about 20 nm are distributed on the $LiFePO_4$/C surface, which is consistent with the analysis from SEM.

Fig. 4 presents the discharge capacities vs. cycle number of the pristine and $LiFePO_4$/C–Sn cathodes at 0.5, 1, 2 and 3 C rate (1 C = 170 mAh g^{-1}) between 2.0 and 4.5 V at 25 °C. With the surface modification of Sn nanoparticles, $LiFePO_4$/C–Sn (0.5 C: 145 mAh g^{-1}; 1 C: 138 mAh g^{-1}; 2 C: 130 mAh g^{-1}; 3 C: 122 mAh g^{-1}, respectively) exhibits higher capacity than Sample A (0.5 C: 140 mAh g^{-1}; 1 C: 128 mAh g^{-1}; 2 C: 110 mAh g^{-1}; 3 C: 90 mAh g^{-1}, respectively), especially at high rate. It is believed that the poor electron transfer activity between $LiFePO_4$ particles results in the inferior electrochemical performance of $LiFePO_4$/C. The increment in discharge capacity suggests that the surface modification with Sn would facilitate the electrochemical insertion/extraction process of Li^+ ion, especially at high rate.

Fig. 5 shows the charge–discharge profiles of cells containing $LiFePO_4$/C and $LiFePO_4$/C–Sn, which is carried out from 0.5 to 3 C between 2.0 and 4.5 V vs. Li^+/Li. Both samples demonstrate typical flat charge/discharge plateaus around 3.4 V, corresponding to the Fe^{2+}/Fe^{3+} redox reaction [13]. It can be seen that as the charge/discharge rate increases, $LiFePO_4$/C–Sn demonstrates a slower enlargement in electrochemical polarization in comparison with the pristine one, shown in Fig. 5(c). Lower polarization suggests

better reaction kinetics. The results indicate that the conductivity between active materials is enhanced by surface modification with metallic Sn, which consequently results in superior rate capability of the cells.

Fig. 6(a) and (b) shows the CV curves of $LiFePO_4$/C and $LiFePO_4$/C–Sn at a scanning rate from 0.05 to 0.4 mV s^{-1}, respectively. It is found that the intensity and area of the redox peaks for both samples increases with the scanning rate. The linear dependence of peak current (i_p) on the square root of scan rate ($v^{1/2}$) is illustrated in Fig. 6(c) and the corresponding lithium diffusion coefficient (D_{Li}) in $LiFePO_4$/C and $LiFePO_4$/C–Sn can be calculated according to the following expression (1) [14]:

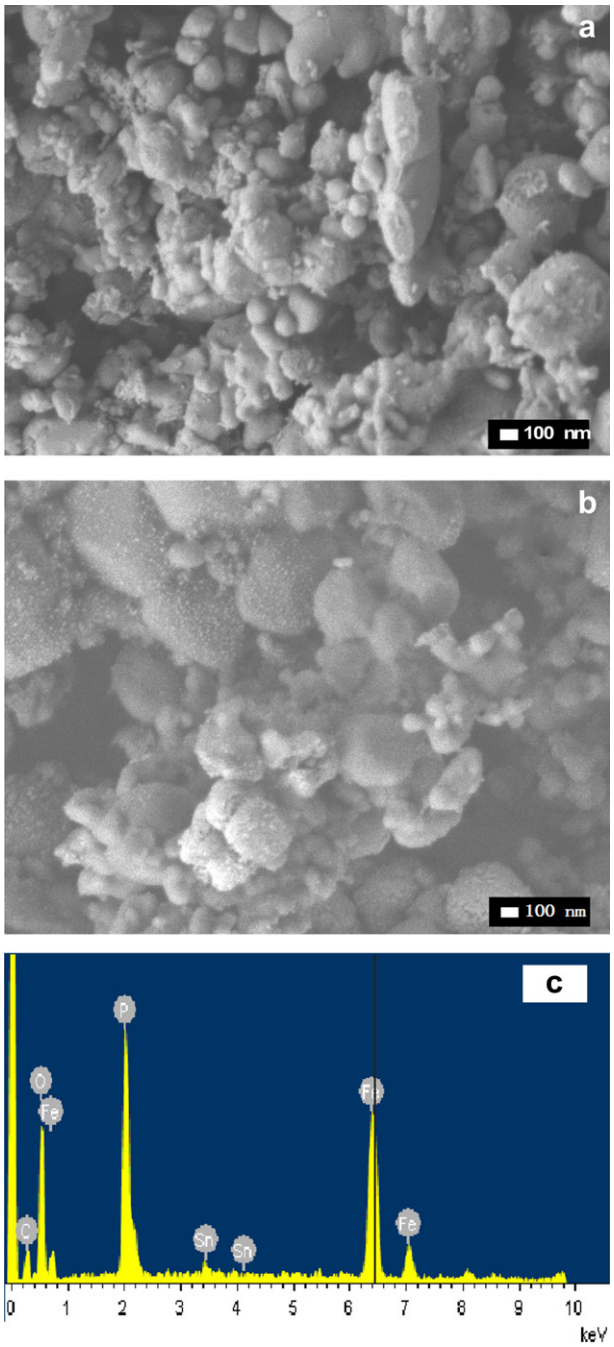

Fig. 2. SEM images of (a) $LiFePO_4$/C, (b) $LiFePO_4$/C–Sn and (c) EDS spectrum of $LiFePO_4$/C–Sn.

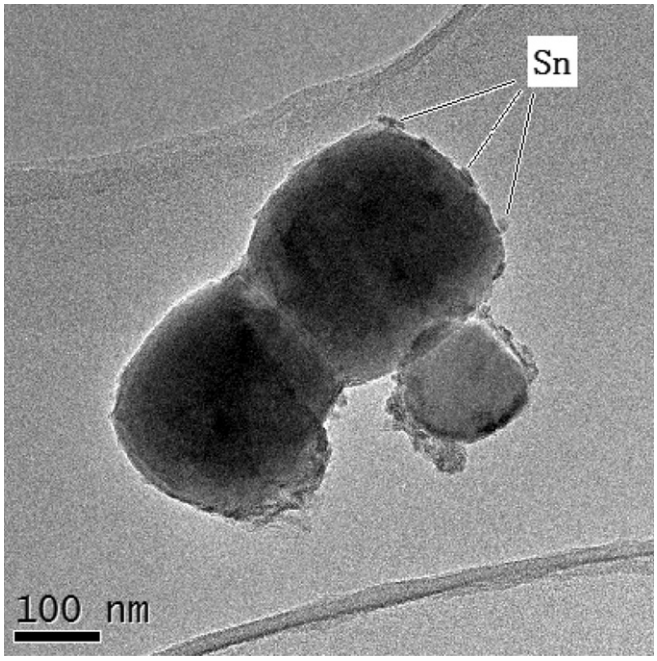

Fig. 3. TEM image of $LiFePO_4$/C–Sn.

$$i_p = \left(2.69 \times 10^5\right) n^{3/2} A D_{Li}^{1/2} C_{Li}^{*} v^{1/2} \quad (1)$$

where i_p is the peak current, n is the charge-transfer number, A is the contact area between cathode and electrolyte, C_{Li}^{*} is the concentration of lithium ions in the cathode and v is the scanning rate, respectively. Based on the slopes of the line in Fig. 6(c), D_{Li} of $LiFePO_4$/C and $LiFePO_4$/C–Sn are calculated as 6.946×10^{-11} cm^2 s^{-1} and 3.598×10^{-10} cm^2 s^{-1}, respectively. The larger D_{Li} of $LiFePO_4$/C–Sn than that of $LiFePO_4$/C reveals that Sn-coating indeed facilitate Li-ion transportation in the electrodes due to the lower surface resistance, which is consistent with the analysis of electrochemical performances.

Fig. 7 shows the capacity cyclability of $LiFePO_4$/C and $LiFePO_4$/C–Sn at 0.5 C at 60 °C, respectively. Compared to the electrochemical

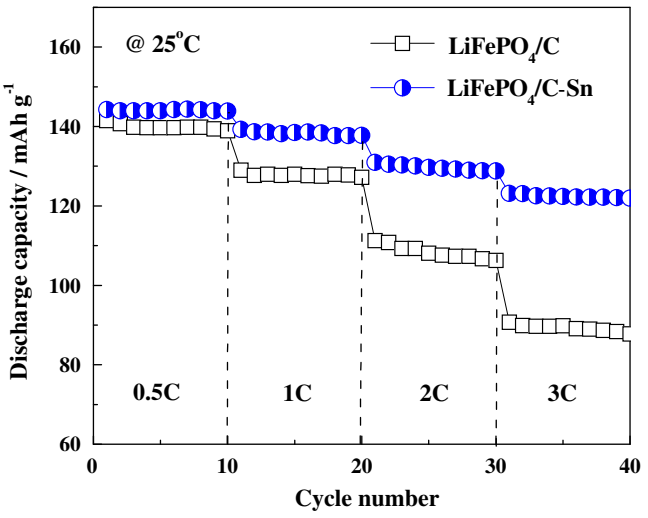

Fig. 4. Rate capability of the pristine $LiFePO_4$/C and $LiFePO_4$/C–Sn composite at 25 °C.

performances at 25 °C, higher capacities are obtained at elevated temperature, which might result from the increased lithium diffusion rate and electron transfer activity [15]. Similar results were reported by some research groups [16,17]. It is obviously observed that $LiFePO_4$/C–Sn exhibits superior capacity cyclability in comparison with $LiFePO_4$/C. The initial discharge capacity of $LiFePO_4$/C–Sn is 154.3 mAh g^{-1} and found to decay gradually with continuous cycling, retaining 147.5 mAh g^{-1} after 130 cycles. The $LiFePO_4$/C also exhibits initial capacity of 150.2 mAh g^{-1} and but its capacity fade faster to 117.8 mAh g^{-1} in totally 130 cycles, suffering a more than 22% capacity loss. It is well-established that the dissolution of Fe from $LiFePO_4$ in $LiPF_6$ electrolyte should be responsible for the severe capacity fade at elevated temperature [6]. The dissolved amount of Fe in $LiFePO_4$/C|Li and $LiFePO_4$/C–Sn|Li cells after 130 cycles at 60 °C was measured by ICP. The dissolved content of Fe in electrolyte for $LiFePO_4$/C and $LiFePO_4$/C–Sn was 18.37 and 13.77 mg L^{-1} respectively, indicating that Sn-coating layer on the $LiFePO_4$/C particle functions as a protective film, which effectively suppresses the surface erosion caused by HF in the

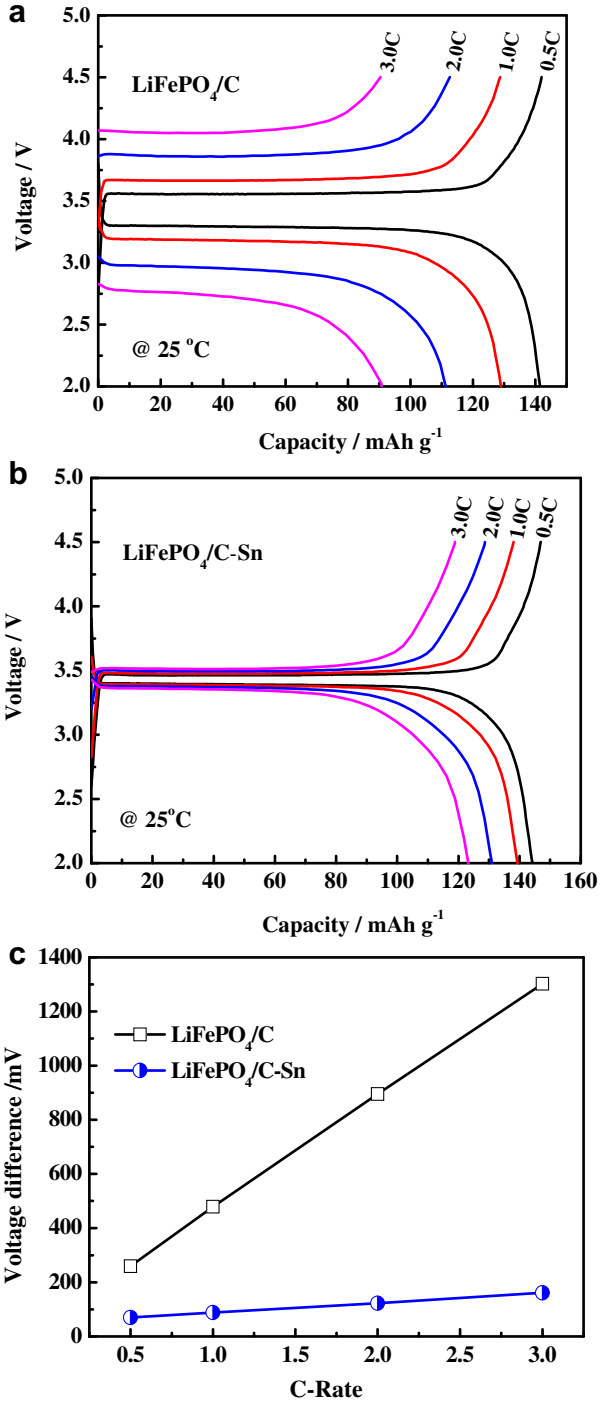

Fig. 5. Charge–discharge profiles of (a) $LiFePO_4$/C and (b) $LiFePO_4$/C–Sn samples at various rate at 25 °C. (c) The relationship of electrochemical polarization and C-rate for both samples.

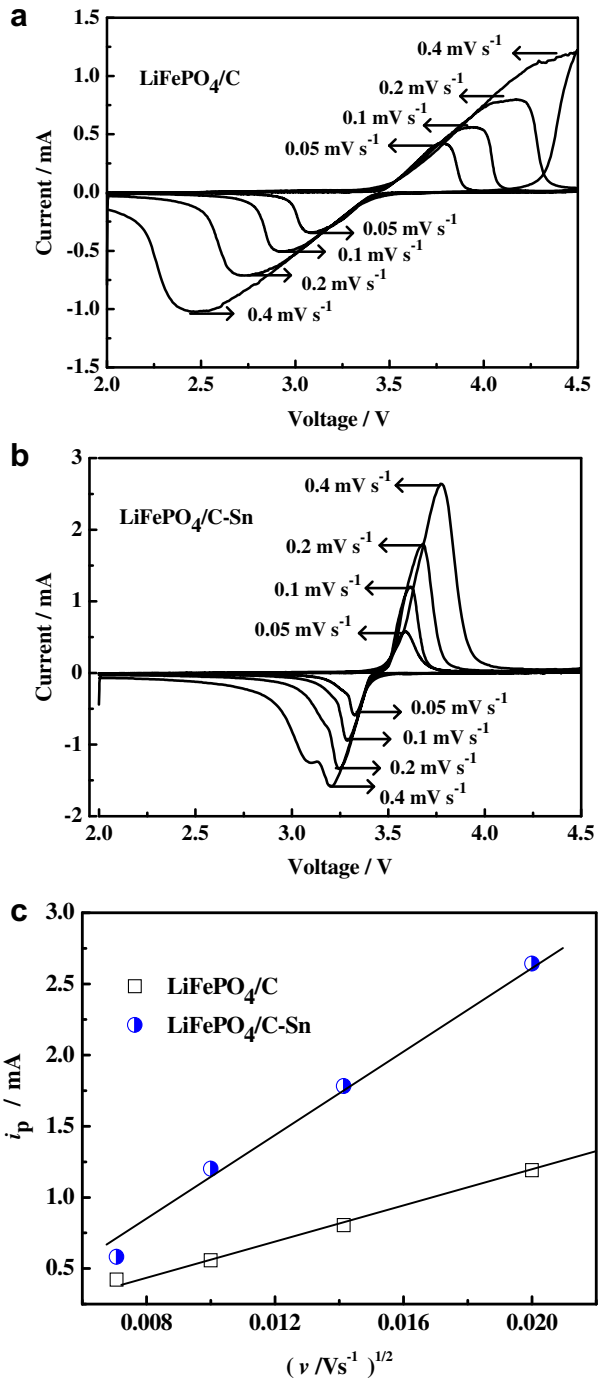

Fig. 6. Cyclic voltammograms of (a) $LiFePO_4$/C and (b) $LiFePO_4$/C–Sn in the voltage range of 2.0–4.5 V at scan rates of 0.05, 0.1, 0.2 and 0.4 mV s^{-1}; (c) The relationship of peak current (i_p) and the square root of scan rate ($v^{1/2}$) for both samples.

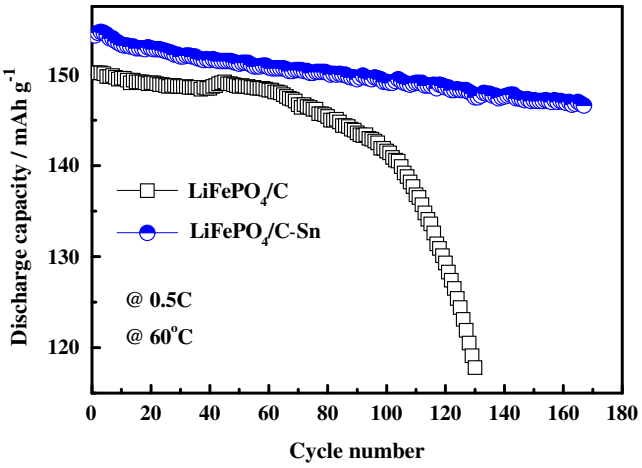

Fig. 7. Cycling performances of $LiFePO_4$/C and $LiFePO_4$/C–Sn at 0.5 C and 60 °C.

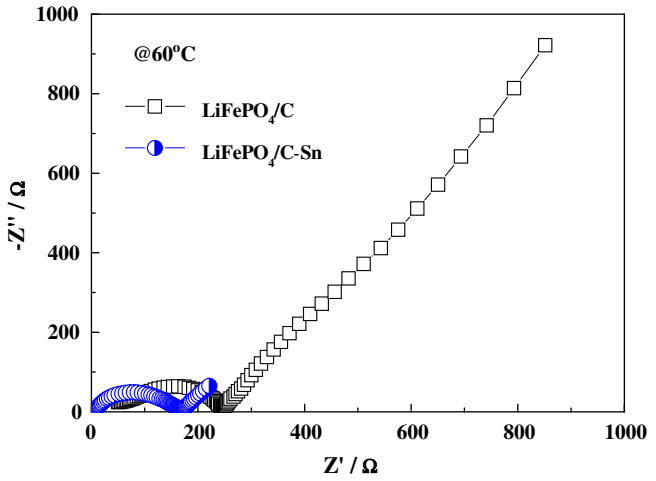

Fig. 9. The EIS profiles of $LiFePO_4$/C and $LiFePO_4$/C–Sn after 130 cycles at 0.5 C at 60 °C.

electrolyte and consequently improve the cyclic stability of the electrode. In addition, the electrochemical reaction between $LiFePO_4$ and $LiPF_6$-based non-aqueous electrolyte is expected to be responsible for the poor performance at elevated temperature [18].

On the other hand, the deposition of organic or inorganic species on the cathode surface, such as LiF, Li_xPF_y and $LiPO_yF_z$, is considered to be responsible for the degradation of the electrochemical performance, which results in a loss of electrical contact within the electrode [19–21]. Based on scattering theory of electron transport across the interface [22], a phenomenological resistance model for $LiFePO_4$/C–Sn composite is set up and a corresponding equivalent circuit between $LiFePO_4$ particles describing these processes is presented in Fig. 8, where R_{LFP}, R_C, R_{Sn} and R_E present $LiFePO_4$ resistance, carbon resistance on the surface of $LiFePO_4$, metallic Sn resistance and the surface resistance arising from the species on the cathode surface. With the presence of high electronic-conductivity Sn on $LiFePO_4$/C particles, the total resistance in parallel is much small in comparison with the pristine one. As a result, the electrochemical performance at elevated temperature was improved.

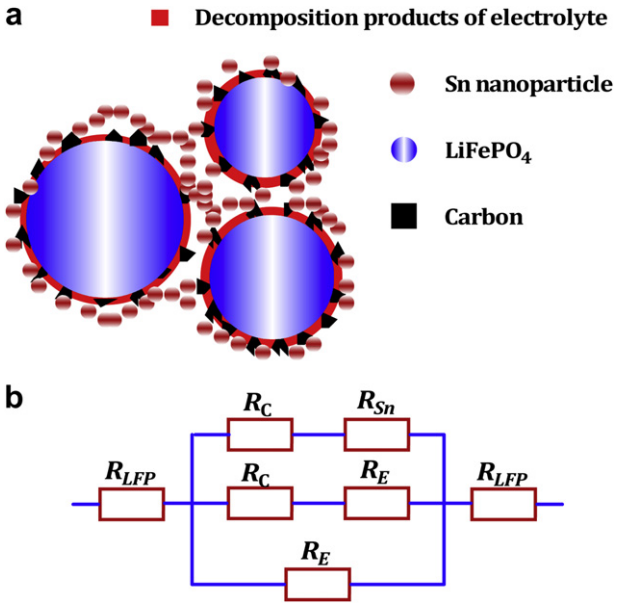

Fig. 8. (a) A phenomenological resistance model and (b) corresponding equivalent circuit between $LiFePO_4$ particle $LiFePO_4$/C–Sn cathode.

Fig. 9 shows typical impedance spectra of the pristine $LiFePO_4$/C and $LiFePO_4$/C–Sn in the fully discharged state after 80 cycles at 1 C rate in 60 °C, respectively. Both EIS profiles are composed of a depressed semicircle at high frequencies and a spike at low frequencies. The intercept of the depressed semicircle at high-frequency region on the real axis is mainly attributed to the charge transfer process [23]. It is evident that $LiFePO_4$/C–Sn has smaller charge-transfer resistance (R_{ct}) than that of the pristine one, which is ascribed to the enhanced electronic contacts between $LiFePO_4$ particles due to the presence of highly conductive Sn. The decrease in R_{ct} probably is expected to overcome the kinetics restrictions in the process of charge/discharge and consequently enlarge the depth of Li-ion insertion/extraction [24].

Excellent low-temperature performance of Li-ion battery is highly desired for specific applications. Fig. 10 presents the rate capability of $LiFePO_4$/C and $LiFePO_4$/C–Sn composites at current density of 0.5, 1, 2 and 3 C at 0 °C. In comparison with the rate capability at 25 °C, the rate capabilities at 0 °C remarkably fall for both composites, resulting from the lower surface reaction kinetics and Li-ion diffusion rate in the electrode [25,26]. In contrast, the beneficial effect of Sn-coating in reducing capacity fading of $LiFePO_4$ at low temperature is obviously observed and $LiFePO_4$/C–Sn (0.5 C: 119 mAh g^{-1}; 1 C: 103 mAh g^{-1}; 2 C: 88 mAh g^{-1}; 3 C:

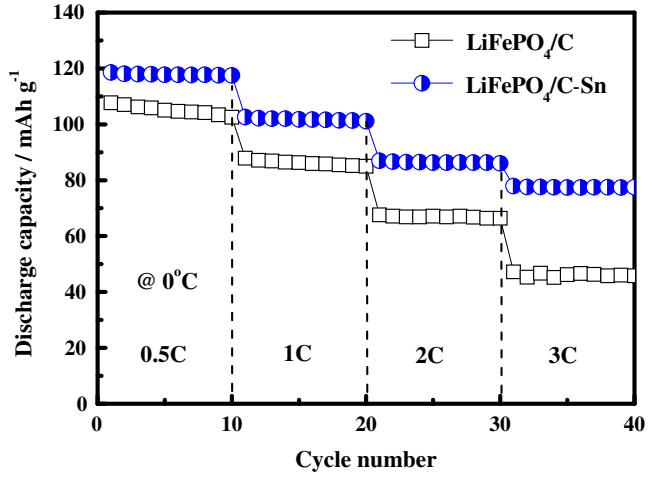

Fig. 10. Rate capability of $LiFePO_4$/C and $LiFePO_4$/C–Sn at current density of 0.5, 1, 2 and 3 C at 0 °C.

78 mAh g^{-1}, respectively) shows better electrochemical performance than that of $LiFePO_4$/C (0.5 C: 106 mAh g^{-1}; 1 C: 88 mAh g^{-1}; 2 C: 67 mAh g^{-1}; 3 C: 47 mAh g^{-1}, respectively).

Fig. 11(a) and (b) presents charge–discharge profiles of $LiFePO_4$/C|Li and $LiFePO_4$/C–Sn|Li cells at 0.5 C rate under different operation temperature between 0 and −30 °C. It is clear that the capacity and the discharge voltage decrease as the operation temperature decreases, which is attributed to the limited electrode kinetics, low Li-ion diffusion, low electrolyte conductivity and high charge-transfer resistance at the electrode/electrolyte interface [15,27,28]. In comparison with above results on the charge–discharge characteristics, the operation temperature has a pronounced effect on the electrochemical performance for $LiFePO_4$/C|Li cell. The results indicate Sn-coating is beneficial in enhancing the electrochemical performances at low temperature.

To get insight into the origin of the superior low temperature of $LiFePO_4$/C–Sn, the EIS measurements are carried out on $LiFePO_4$/C and $LiFePO_4$/C–Sn cathode materials at the 3rd full charge state from 0 °C to −30 °C, shown in Fig. 12. It is clearly seen that the impedance spectrum is composed of two partially overlapped semicircles at high and medium frequencies, and an oblique straight line at low frequencies. The obtained results suggest that the cell electrochemical resistance results from the complicated electrochemical reactions over the cathode surface and the corresponding equivalent circuit is present in Fig. 12(c). According to the

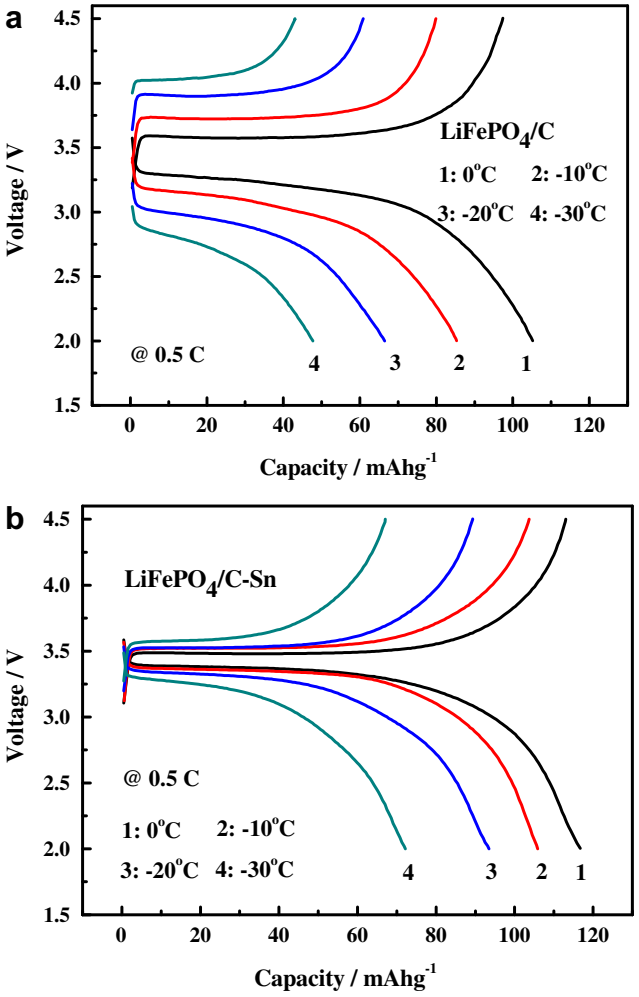

Fig. 11. Charge/discharge voltage profiles of $LiFePO_4$/C and $LiFePO_4$/C–Sn at 0.5 C rate under different operation temperature between 0 and −30 °C.

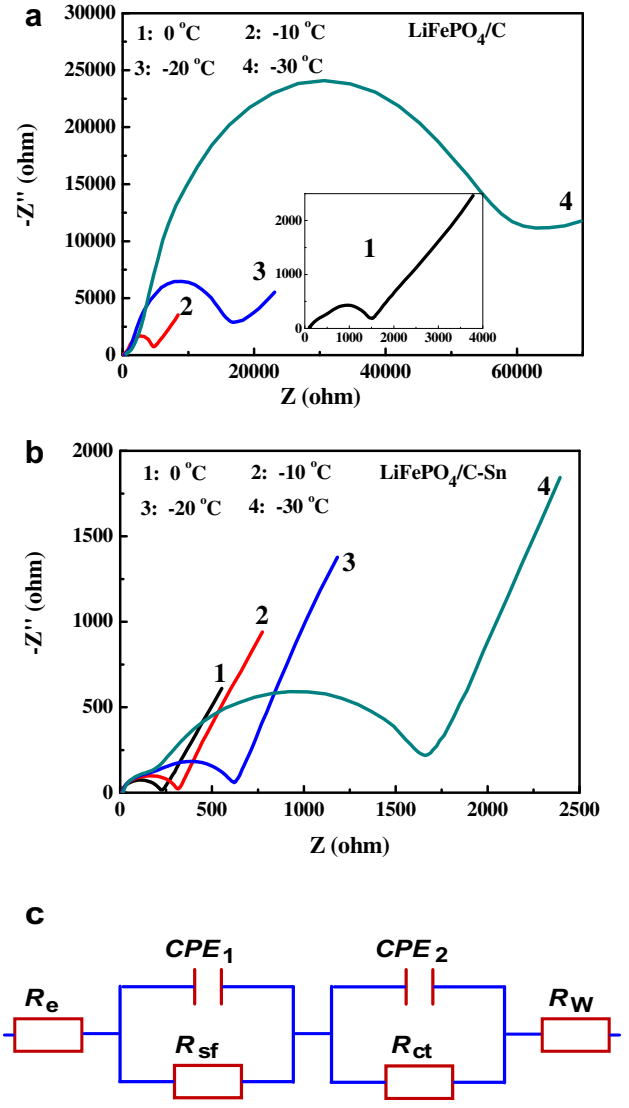

Fig. 12. EIS for (a) LiFePO4/C and (b) LiFePO4/C–Sn at the 3rd full charge state at different operation temperatures and (c) equivalent circuit used for fitting the experimental impedance data.

literature [29], R_b, represents the resistance including the electrolyte, solution resistance and electrode; R_{sf} is the diffusion resistance of Li^+ ions through SEI layer; R_{ct} is the charge transfer resistance and R_w is Warburg impedance related to the lithium ions diffusion in the active material, respectively. The impedance data are analyzed with Z-view software. In comparison with $LiFePO_4$/C–Sn, $LiFePO_4$/C exhibits more pronounced effect on charge-transfer resistance in electrode–electrolyte interface as the operation temperature falls down. Higher R_{ct} generally corresponds to a slower kinetics of the faradic reaction [30], which adequately explains why the low-temperature performance of $LiFePO_4$/C–Sn is superior to $LiFePO_4$/C. The activation energy (ΔG) of lithium-ion insertion/extraction for $LiFePO_4$/C and $LiFePO_4$/C–Sn can be calculated by the following equation,

$$\log R_{ct} = \log A + \frac{\Delta G - R}{2.303RT} \quad (2)$$

where ΔG is the activation energy, T is the absolute temperature, R is the gas constant, and A is a temperature-independent constant.

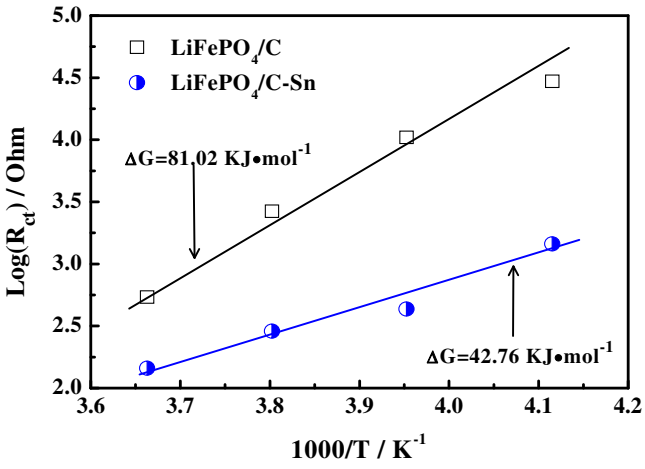

Fig. 13. Profile of log (R_{ct}) vs. temperature for LiFePO4/C and LiFePO4/C–Sn.

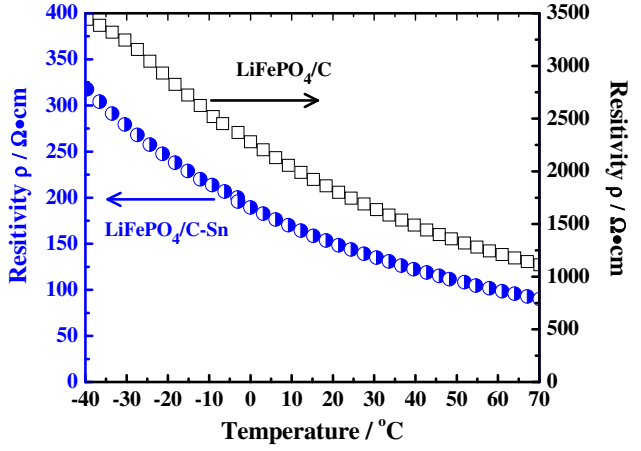

Fig. 14. The temperature dependence of the resistivity for $LiFePO_4$/C and $LiFePO_4$/C–Sn measured by standard four-point probe technique.

Fig. 13 presents the temperature dependence of log R_{ct} in the temperature range from 0 °C to −30 °C and the ΔG for $LiFePO_4$/C and $LiFePO_4$/C–Sn are accordingly calculated as 81.02 KJ mol^{-1} and 42.76 KJ mol^{-1}, respectively. Lower activation energy directly corresponds to faster Li-ion diffusion [31]. The obtained results further confirm that surface modification with high conductivity Sn could significantly facilitate the kinetics for lithium diffusion and the charge transfer reaction, especially at low temperature.

Fig. 14 shows the temperature dependence of the resistivity for $LiFePO_4$/C and $LiFePO_4$/C–Sn measured by standard four-point probe technique between −40 °C and 70 °C, where the testing sheets were made by pressing as-prepared powder under 20 MPa. Obviously, $LiFePO_4$/C–Sn has much smaller resistivity than that of $LiFePO_4$/C in the whole operation temperature range, indicating that the incorporation of Sn nanoparticles is an effective way of increasing the conductivity of the composite and facilitates the electron transport in the electrochemical lithium insertion/extraction process. As a result, the electrochemical performances were significantly improved.

4. Conclusions

Nano-sized Sn particles were successfully deposited on the surfaces of $LiFePO_4$/C particles by a facilitate electroless deposition (ED) process. Compared to the pristine $LiFePO_4$/C, the Sn-coated $LiFePO_4$/C exhibits superior electrochemical performances in a wide operation temperature range. The obtained results reveal that the presence of metallic Sn on $LiFePO_4$/C surface plays an important role in decreasing the interfacial impedance, enhancing lithium diffusion rate and suppressing the dissolution of Fe from active materials in the $LiPF_6$ based electrolyte.

Acknowledgments

This work was supported by a grant from National Science Foundation for Young Scholars (No. 11004032) and Natural Science Foundation of China (No.11074039), and the National Key Project for Basic Research of China (No. 2011CBA-00200).

References

[1] M.M. Doeff, J.D. Wilcox, R. Kostecki, G. Lau, J. Power Sources 163 (2006) 180.
[2] S. Zhang, K. Xu, T. Jow, J. Power Sources 159 (2006) 702.
[3] C.W. Ong, Y.K. Lin, J.S. Chen, J. Electrochem. Soc. 154 (2007) A527.
[4] J. Ying, M. Lei, C. Jiang, C. Wan, X. He, J. Li, L. Wang, J. Ren, J. Power Sources 158 (2006) 543.
[5] P. Reale, S. Panero, B. Scrosati, J. Garche, M. Wohlfahrt-Mehrens, M. Wachtler, J. Electrochem. Soc. 151 (2004) A2138.
[6] H.H. Chang, H.C. Wu, N.L. Wu, Electrochem. Commun. 10 (2008) 1823.
[7] Y. Liu, C. Mi, C. Yuan, X. Zhang, J. Electroanal. Chem. 628 (2009) 73.
[8] C. Mi, Y. Cao, X. Zhang, X. Zhao, H. Li, Powder Technol. 181 (2008) 301.
[9] G.M. Song, Y. Wu, Q. Xu, G. Liu, J. Power Sources 195 (2010) 3913.
[10] J. Ni, M. Morishita, Y. Kawabe, M. Watada, N. Takeichi, T. Sakai, J. Power Sources 195 (2010) 2877.
[11] F. Croce, A. D'Epifanio, J. Hassoun, A. Deptula, T. Olczac, B. Scrosati, Electrochem. Solid-State Lett. 5 (2002) A47.
[12] H. Liu, J. Xie, K. Wang, Solid State Ionics 179 (2008) 1768.
[13] H.C. Wu, C.Y. Su, D.T. Shieh, M.H. Yang, N.L. Wu, Electrochem. Solid-State Lett. 9 (2006) A537.
[14] Y. Jin, C.P. Yang, X.H. Rui, T. Cheng, C.H. Chen, J. Power Sources 196 (2011) 5623.
[15] W.J. Zhang, J. Power Sources 196 (2011) 2962.
[16] A.S. Andersson, J.O. Thomas, L. Kalska, B. Haggstrom, Electrochem. Solid-State Lett. 3 (2000) 66.
[17] M. Takahashi, S. Tobishima, K. Takei, Y. Sakurai, J. Power Sources 97-98 (2001) 508.
[18] S.B. Lee, S.H. Cho, V. Aravindan, H.S. Kim, Y.S. Lee, Bull. Korean Chem. Soc. 30 (2009) 2223.
[19] N. Dupré, J.F. Martin, J. Degryse, V. Fernandez, P. Soudan, D. Guyomard, J. Power Sources 195 (2010) 7415.
[20] L. Castro, R. Dedryvere, J.-B. Ledeuil, J. Breger, C. Tessier, D. Gonbeau, J. Electrochem. Soc. 159 (2012) A357.
[21] R. Dedryvere, M. Maccario, L. Croguennec, F. Le Cras, C. Delmas, D. Gonbeau, Chem. Mater. 20 (2008) 7164.
[22] Z.G. Huang, Z.G. Chen, K. Peng, D.H. Wang, F.M. Zhang, W.Y. Zhang, Y.W. Du, Phys. Rev. B 69 (2004) 094420.
[23] H. Liu, G.X. Wang, D. Wexler, J.Z. Wang, H.K. Liu, Electrochem. Commun. 10 (2008) 165.
[24] J.M. Cao, Y. Qu, R.S. Guo, Electrochim. Acta 67 (2012) 152.
[25] J. Yao, F. Wu, X. Qiu, N. Li, Y. Su, Electrochim. Acta 56 (2011) 5587.
[26] Y. Zhou, C. Gu, J. Zhou, L. Cheng, W. Liu, Y. Qiao, X. Wang, J. Tu, Electrochim. Acta (2011) 5054.
[27] X.Z. Liao, Z.F. Ma, Q. Gong, Y.S. He, L. Pei, L.J. Zeng, Electrochem. Commun. 10 (2008) 691.
[28] S. Franger, C. Benoit, C. Bourbon, F. Le Cras, J. Phys. Chem. Solids 67 (2006) 1338.
[29] H.M. Wu, I. Belharouak, A. Abouimrane, Y.-K. Sun, K. Amine, J. Power Sources 195 (2010) 2909.
[30] X.H. Rui, Y. Jin, X.Y. Feng, L.C. Zhang, C.H. Chen, J. Power Sources 196 (2011) 2109.
[31] M. Okubo, Y. Tanaka, H.S. Zhou, I. .Honma, J. Phys. Chem. B 113 (2009) 2840.